ISBN: 978-3-95450-222-6 ISSN: 2673-5350 doi:10.18429/JACoW-IBIC2020-THPP33

SIMULATION METHODS FOR TRANSVERSE BEAM SIZE MEASUREMENTS USING THE HETERODYNE NEAR FIELD SPECKLES OF HARD X-RAYS

A. Goetz*, D. Butti, S. Mazzoni, G. Trad, CERN, Geneva, Switzerland
U. Iriso, A. A. Nosych, L. Torino, ALBA-CELLS, Cerdanyola Del Vallés, Spain
B. Paroli, M. A. C. Potenza, M. Siano, L. Teruzzi, Università degli Studi di Milan, Milano, Italy

Abstract

Heterodyne Near Field Speckles (HNFS) is a special type of interferometry technique where radiation is scattered by nanoparticles suspended in a medium. The weak scattered waves and the intense transmitted beam form an interference pattern, which is modulated by the spatial coherence of the radiation and by the scattering properties of the nanoparticles. The random superposition of many such interference patterns results in a speckle field from which the spatial coherence of the radiation, thus the transverse beam profile, can be determined. In this contribution we present approaches for simulating the HNFS patterns from hard X-ray radiation and compare then with data from experiments at the ALBA synchrotron.

INTRODUCTION

With photon beam energies of up to 100 keV in combination with an unprecedented brightness and manifold focusing possibilities, third-generation light sources have become an indispensable tool for modern nanoscale science [1]. Precise knowledge about the coherence properties of the synchrotron radiation offers a wide range of technical applications. It is at the basis of many coherence-based techniques [2], and can also give insights into the transverse particle beam distribution. As such, coherence measurements are currently studied in the context of a non-invasive transverse beam profile monitor for the Future Circular Collider, FCC-ee [3].

In this framework, the Heterodyne Near Field Speckle method is particularly appealing since it allows to access the 2D transverse coherence properties of an X-ray beam without the need of any dedicated X-ray optics. Originally introduced in the optical domain as a particle-sizing technique by Giglio et al. [4], it has been recently extended by Alaimo et al. in 2009 to the characterization of the spatial coherence properties of undulator X-ray beams [5]. An extensive study on the application of the HNFS method to spatial and temporal coherence measurements of visible synchrotron radiation has been reported in 2016 by Siano et al. [6].

In spite of its experimental success, the method still lacks robust simulations that take into account the peculiar features of undulator radiation and the optical properties of the scattering particles. In this contribution we aim to compare two different approaches of simulating X-ray Heterodyne Near Field Speckles.

* alexander.goetz@cern.ch

THEORY OF THE HNFS

As far as transverse coherence is concerned, the radiation emitted by a single electron moving through an undulator is fully coherent. A statistical ensemble of electrons, with a Gaussian shaped profile with horizontal size σ_x and vertical size σ_y, gives rise to coherence areas of size $\sigma_{vcz,x/y}$ at a distance z from the undulator center. These coherence areas follow the Van Cittert and Zernike theorem [7, 8]:

$$\sigma_{vcz,x/y} = \frac{\lambda z}{2\pi\sigma_{x/y}} \tag{1}$$

where $\sigma_{\mathrm{vcz,x/y}}$ is the transverse coherence length along the *x/y* direction, λ is the radiation wavelength, z is the distance from the center of the undulator and $\sigma_{x/y}$ is the rms size of the electron beam along the corresponding direction. When such a partially coherent wavefront impinges onto a suspension of particles with diameter d (a colloidal suspension), the synchrotron radiation is scattered. The weakly scattered spherical waves interfere with the intense trans-illuminating beam to generate Heterodyne Near Field Speckles [6]. The near field conditions, which are eponymous to this technique, require to measure the resulting interference pattern at distances z_2 downstream the scattering plane fulfilling

$$z_2 < \frac{\sigma^2_{vcz,x/y}}{\lambda} \tag{2}$$

Let us write the field of the synchrotron radiation produced by a given electron with index l as $E_l(\mathbf{x})$, the positions of the colloids with index j as $\mathbf{x}_j$ and their scattering amplitude function as $S(\mathbf{x})$. The interference image is then given by

$$I(\mathbf{x}) = \sum_l \left| \sum_j E_l(\mathbf{x}) + E_l(\mathbf{x}_j) \cdot S(\mathbf{x} - \mathbf{x}_j) \right|^2 \tag{3}$$

The individual electrons are assumed to be uncorrelated, which is why they are summed outside of the absolute square. The intensity captured by a sensor is then Fourier transformed and the corresponding power spectrum $I(\mathbf{q})$ is computed with a spatial frequency variable $\mathbf{q}$. The power spectrum shows fringes that decay due to the scattering amplitude function (the particle form factor) $S(\mathbf{q})$, the spatial coherence of the radiation $C(\mathbf{q})$ and the optical transfer function $H(\mathbf{q})$. It is additionally shaped by the Talbot oscillations $T(\mathbf{q})$ and exhibits a noise pedestal $P(\mathbf{q})$ [6]:

$$I(\mathbf{q}) = S(\mathbf{q}) \cdot T(\mathbf{q}) \cdot C(\mathbf{q}) \cdot H(\mathbf{q}) + P(\mathbf{q}) \tag{4}$$

ISBN: 978-3-95450-222-6 ISSN: 2673-5350 doi:10.18429/JACoW-IBIC2020-THPP33

Notice how the first four terms would appear in the form of a convolution in direct space, whereas they are represented by a multiplication in the reciprocal space, which makes it easy to examine individual terms. In particular, the envelope of the Talbot oscillations gives access to the 2D transverse coherence properties of the incoming undulator radiation. The 2D transverse profile of the electron beam is then retrieved by recalling the Van Cittert and Zernike theorem.

SIMULATION A: USING SRW AS A MAXWELL EQUATION SOLVER

First published in 1997 at the ESRF [9], Synchrotron Radiation Workshop (SRW) is an algorithm for the numerical evaluation of synchrotron radiation from an arbitrary magnet including undulators in synchrotrons. It is well established in the accelerator community and it is widely used for studies on synchrotron radiation. Beside calculations of the electric field, it also allows this field to be propagated through drift spaces, lenses, apertures or arbitrary 2D phase shifting and attenuating elements [9].

In our simulations, as a first step a set of electrons at positions $\mathbf{x}_l$ is chosen, representing the transverse beam profile. Using this profile the SRW code is used to create a synchrotron radiation wavefront given the specification of the NCD-SWEET undulator beamline at ALBA reported in Table 1.

Table 1: ALBA-CELLS NCD-SWEET Undulator Parameter

parameter	value
beam size σ_x	130 µm
beam size σ_y	6.5 µm
beam divergence σ'_x	47.6 µrad
beam divergence σ'_y	11.9 µrad
beam energy	2.96 GeV
undulator number of periods	92
undulator period length	21.6 mm
monochromator energy	12.4 keV
monochromaticity of radiation $\Delta E/E$	1e-4
distance from undulator to sample z	33 m

At a radiation energy of 12.4 keV, the silica colloids have a refractive index of $n-1 = \delta+\beta i = 3.59e{-}6{+}1.98e{-}8i$ [10]. While the real part causes a phase shift and is thus responsible for refraction, the imaginary part leads to absorption. The latter has been neglected in our simulations since $\beta \ll \delta$. For the simulation it is assumed that each colloid in the suspension imposes a phase shift on the wavefront. This phase shift is scaled according to the effective path length through the spherical structure of the colloids, yielding a phase shift profile for all the colloid positions $\mathbf{x}_j$. A Heaviside function is used to suppress negative values in the square root:

$$\Delta\phi(\mathbf{x}) = \sum_j \sqrt{1-\left(\frac{|\mathbf{x}-\mathbf{x}_j|}{R}\right)^2}\cdot\frac{2R\delta\omega}{c}\cdot H(R-|\mathbf{x}-\mathbf{x}_j|) \tag{5}$$

This phase shift mask is applied to the wavefront by multiplying it with $e^{i\Delta\phi}$ and propagated with SRW until the plane z_2 where the image is formed. The intensity distribution at this plane is then computed as the squared modulus of the electric field. This process is repeated for each radiating electron. In a final step all the images are summed to produce the final speckle pattern. The power spectrum of the resulting speckle image is shown in Fig. 1.

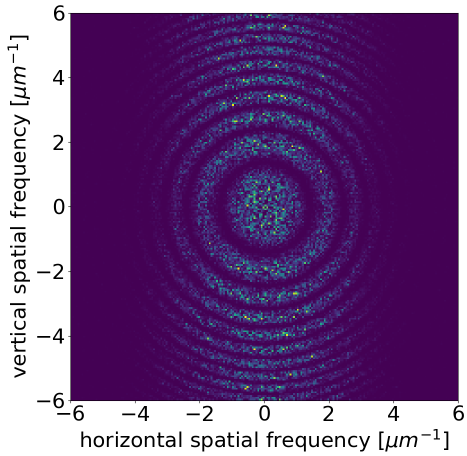

Figure 1: 2D power spectrum of the simulated speckle pattern at distance $z_2 = 10$ cm after the colloids. With reference to Eq. (1), the plot reveals the wide beam size in the horizontal and the narrow beam size in the vertical plane.

In order to extract the coherence properties of the incoming X-ray beam along the horizontal and vertical direction, crosscuts are taken through the center of the 2D power spectrum along the horizontal and vertical axis, respectively. The accuracy of these crosscuts can be further increased by calculating the angular average over double-cone sectors for each plane.

The computational effort is usually quite high for this type of simulation. For about 1000 macro-electrons, with which a good reproduction of the transverse beam profile can be achieved, about 300 CPUH and a diskspace of about 1 TB is necessary.

SIMULATION B: USING FOURIER OPTICS IN HETERODYNE CONDITIONS

Let $e_t(\mathbf{x},z)$ and $e_s(\mathbf{x},z)$ denote the intense transmitted field and the total faint scattered radiation, respectively. The latter can be expressed as $e_s = \sum_{j=1}^{N} e_{s,j}$, where $e_{s,j}$ is the spherical wave scattered by the j-th particle with position $\mathbf{x}_j$ and N is the total number of scattering centers. Both e_t and $e_{s,j}$ can be related to the incident beam e_0:

$$\begin{aligned} e_t(\mathbf{x},z) &= e_0(\mathbf{x})\exp(ikz) \\ e_{s,j}(\mathbf{x},z) &= e_0(\mathbf{x}_j)\frac{S(\theta_j)}{ikz}\exp(ikz)\exp\left(\frac{k|\Delta\mathbf{x}_j|^2}{2z}\right), \end{aligned} \tag{6}$$

ISBN: 978-3-95450-222-6 ISSN: 2673-5350 doi:10.18429/JACoW-IBIC2020-THPP33

where $k = 2\pi/\lambda$, $\Delta\mathbf{x}_j = \mathbf{x} - \mathbf{x}_j$ and $S(\theta_j)$ is the particle form factor as a function of the scattering angle $\theta_j = \arctan(|\Delta\mathbf{x}_j|/z)$. Under heterodyne conditions $|e_s| \ll |e_t|$ [6], the self-beating (homodyne) term $|e_s|^2$ of the scattered field can be neglected and the speckle intensity distribution I in Eq. (3) is given by the sum of many independent single-particle contributions s_j [6]:

$$I(\mathbf{x}, z) = |\langle e_0(\mathbf{x})\rangle|^2 + \sum_{j=1}^{N} s_j(\mathbf{x}, z)\,, \tag{7}$$

where angular brackets denote ensemble averages over many iterations of the incident field [8] and s_j describes the interference between the scattered spherical wave and the transmitted partially coherent beam:

$$s_j(\mathbf{x}, z) = \frac{2}{kz}|J(\Delta\mathbf{x}_j)| \cdot |S(\theta_j)| \cdot \cos\left[\frac{k}{2z}|\Delta\mathbf{x}_j|\right]. \tag{8}$$

In Eq. (8), $J(\Delta\mathbf{x}) = \langle e_0(\mathbf{x}+\Delta\mathbf{x})e_0^*(\mathbf{x})\rangle$ is the Mutual Coherence Function (MIF) [8] describing the transverse coherence of the incoming X-ray beam. We emphasize how Eq. (7) and Eq. (8) provide the exact, rigorous solution to the sum over many independent electrons in Eq. (3). By this we mean that computations based on Eq. (3) give the same results as Eq. (8) for a single scattering particle.

In Eq. (8), it is only required to accurately characterize J and S. The former is related to the Fourier transform of the source intensity distribution (Van Cittert and Zernike theorem) [8] and it is therefore easily computed for a Gaussian electron beam. The latter can be calculated by means of the exact Mie theory of light scattering for spherical particles [11]. Furthermore, for small scatterers with $d = 500$ nm or smaller, $S(\theta_j) \sim S(0)$ to a good approximation, which greatly simplifies the task.

The method is sketched in Fig. 2. Remarkably, the computation time is independent of N and it is only limited by the size of the simulation mesh. Furthermore, the required storage space is reduced to a minimum, since the output of the simulation is typically a single raw file of $\sim 10^6$ double values.

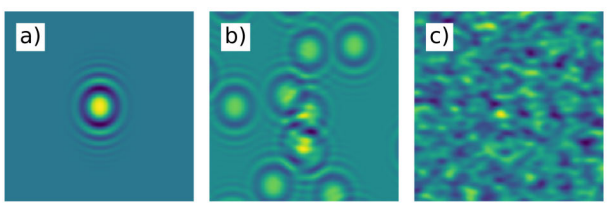

Figure 2: A sketch of simulation method B. (a) Single-particle interference image as in Eq. (8). (b) Few-particle case. (c) Many-particle (speckle) case.

The simulated speckle fields are then convoluted with the Point Spread Function (PSF) of the optical system (related to the Fourier transform of the term $H(q)$ in Eq. (4)) to account for resolution losses. We can also benefit from the linearity of Eq. (7) with respect to the single-particle contribution to perform such a convolution operation directly on Eq. (8), thus preventing aliasing artifacts in the simulated images.

The only free parameter is the mean intensity value $|\langle e_0\rangle|^2$ of the incoming beam. We typically assume $|\langle e_0\rangle|^2 = 1$ throughout the simulation, and then scale the mean value of the overall intensity distribution to match experimental data. This also provides an efficient way to account for the quantum efficiency of the detector and the read-out gain.

COMPARISON WITH EXPERIMENTAL DATA

One of the biggest challenges of the experiment is to measure the transfer function $H(q)$. It is mainly influenced by the scintillator and the microscope objective setup, which converts the X-rays into visible light and projects it onto the sensor. Additionally to this calibration curve, a water sample is imaged in order to find the pedestal, on top of which the signal is expected to appear. Both curves have been experimentally determined and properly accounted for in the imaging process of the simulated speckle patterns.

A comparison between the simulated horizontal profile of the heterodyne speckle power spectrum and actual data is reported in Fig. 3.

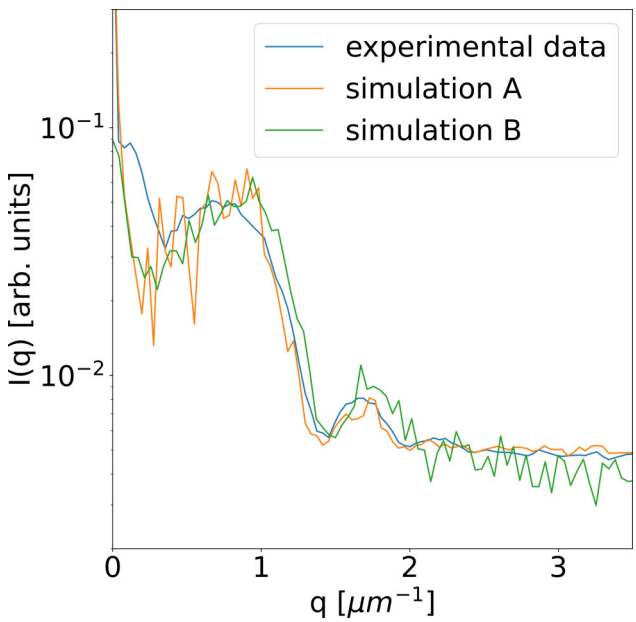

Figure 3: The power spectrum of the experimental data is compared with simulations A and B for the ALBA-CELLS NCD-SWEET in a distance $z_2 = 0.2$ m, at a radiation wavelength of $\lambda = 0.1$ nm, for the horizontal plane.

Agreement is found between simulations and the measured curve. Remarkably, simulation A and simulation B yield the same results, in spite of the fundamentally different approaches adopted. The raw speckle pattern are presented in Fig. 4 for completeness.

ISBN: 978-3-95450-222-6 ISSN: 2673-5350 doi:10.18429/JACoW-IBIC2020-THPP33

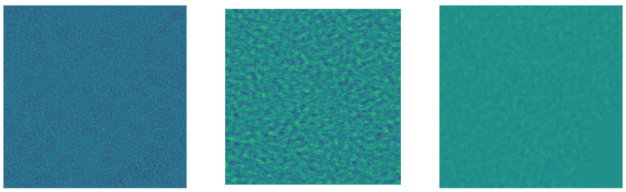

Figure 4: From left to right, the raw speckles pattern of simulation A, simulation B and the experimental data are shown.

CONCLUSION

The main advantage of simulation A is the precise calculation of the synchrotron radiation of an arbitrarily parameterized undulator, while simulation B is based on the assumption that the Van Cittert and Zernike theorem holds true for a given magnetic structure. Simulation B neglects the homodyne terms of the scattered waves, while simulation A takes them into account. Notice how this is not actually necessary, thanks to the heterodyne conditions of the technique. As for the scattering sample, simulation A relies on the approximation of two dimensional phase shifting obstacles, while simulation B applies the exact Mie formulas for spherical particles. Concerning the computational efficiency, simulation A scales linearly with the number of radiation electrons, while simulation B overcomes this issue by computing the radiation MIF through the Van Cittert and Zernike theorem. Finally, the computational complexity does not depend on the number of colloids for both simulation techniques.

We have tested the two simulation methods against real data from an undulator X-ray beam at the NCD-SWEET beamline at ALBA. Simulations compare well with actual measurements, especially regarding the horizontal profiles of the heterodyne speckle power spectrum. This proves the validity of the Van Cittert and Zernike theorem in describing the coherence properties of the incoming X-ray wavefronts. Additional investigations, both numerically and experimentally, are ongoing for the vertical transverse coherence length.

REFERENCES

[1] D. Mills, *Third Generation Hard X-ray Synchrotron Radiation Sources*. New York, USA: John Wiley and Sons, 2002.

[2] K.A. Nugent, "Coherent methods in the X-ray sciences", *Advances in Physics*, vol. 59, pp. 1–99, 2010. doi:10.1080/00018730903270926

[3] M. Benedikt *et al.*, "FCC-ee: The Lepton Collider", *Eur. Phys. J. Spec. Top.*, vol. 288, pp. 425–426, 2019. doi:10.1140/epjst/e2019-900045-4

[4] D. Brogioli, A. Vailati, M. Giglio, "Heterodyne near-field scattering", *Appl. Phys. Lett.*, vol. 81, p. 4109, 2002. doi:10.1063/1.1524702

[5] M. D. Alaimo, M. A. C. Potenza, M. Manfredda, G. Geloni, M. Sztucki, T. Narayanan, and M. Giglio, "Probing the Transverse Coherence of an Undulator X-Ray Beam Using Brownian Particles", *Phys. Rev. Lett.*, vol. 103, p. 194805, 2009. doi:10.1103/physrevlett.103.194805

[6] M. Siano *et al.*, "Transverse Beam Size Diagnostics using Brownian Nanoparticles at ALBA", in *Proc. IBIC'16*, Barcelona, Spain, Sep. 2016, pp. 248–252. doi:10.18429/JACoW-IBIC2016-MOPG73

[7] M. Born and E. Wolf, *Principles of Optics*. Cambridge, England: Cambridge University Press, 1999.

[8] J. W. Goodman, *Statistical Optics*. New York, USA: Wiley-Interscience, 2000.

[9] O. Chubar and P. Elleaume, "Accurate and Efficient Computation of Synchrotron Radiation in the Near Field Region", in *Proc. EPAC'98*, Stockholm, Sweden, Jun. 1998, paper THP01G, pp. 1177–1179.

[10] S. Kuznetsov, "X-Ray Optics Calculator", IMT RAS, Chernogolovka, Russia, http://purple.ipmt-hpm.ac.ru/xcalc/xcalc_mysql/ref_index.php

[11] H.C. Hulst, *Light Scattering by Small Particles*. New York, USA: John Wiley and Sons, 1957.